Tellus (1985), *37A*, 249–257

On hysteresis-like effects in orographically forced models

By ERLAND KÄLLÉN *Department of Meteorology*[1], *University of Stockholm, Arrhenius Laboratory, S-106 91 Stockholm, Sweden*

(Manuscript received June 13; in final form November 21, 1984)

ABSTRACT

Time integrations with an orographically forced high resolution, barotropic model have shown hysteresis-like behaviour. The orography consists of an isolated, mid-latitude hump and the flow is forced with a solid body rotation. For an increasing forcing, a marked instability is found, but it is not connected with a bifurcation, as the model only has one stable equilibrium state. It is found that the instability is coupled to orographic effects and that a slow time evolution of the flow is required for its existence. It is argued that the hysteresis-like effects found here are perhaps more relevant to atmospheric behaviour than bifurcations leading to multiple equilibria.

1. Introduction

A number of recent studies have dealt with non-linear effects in orographically forced, barotropic models. Studies of low-order systems (Charney and de Vore (CdV), 1979; Davey, 1980; Källén, 1981) have revealed that through the combined effects of orographic forcing and dissipation, the fluid can maintain several steady-states for a given set of external conditions. Some of these steady-states are stable and in particular one may find two stable states where the orography acts as a strong and a weak wave generator, respectively. The state in which the orography acts as a strong-wave generator has been associated with a blocked flow in the atmosphere.

The dynamics of a low-order model is severely restricted by the fact that the kinetic energy is contained in only a few scales of motion. Non-linear interactions with larger and smaller scales of motion may give rise to energy transfers which prevent the formation of multiple steady-states for a given set of external conditions. It has, however, been shown by several investigators that if the orographic forcing and the dissipation mechanism are sufficiently strong, a bifurcation leading to the formation of multiple steady-states can still be found (Davey, 1981; Källén, 1982). The main factor responsible for the bifurcation is a resonance occurring when the Rossby wave generated by the orography becomes stationary. The strength of zonal flow over the orography is determined by the externally-prescribed driving of the zonal flow and the drag exerted by the mountain on the zonal flow. If the zonal flow is close to but just above a resonant value, we may have a positive feedback where a large amplitude wave will increase the drag which in turn slows down the zonal flow. The zonal flow then comes even closer to a resonant value which further enhances the wave amplitude and so on. The dissipation puts a limit to the growth of the wave amplitude and we may thus find a balanced state close to resonance. It may also be possible, with the same external driving, to have a balanced state where the wave and thus the mountain drag is weak and the zonal flow is strong. The strong zonal flow is then far removed from resonance and the weak wave amplitude is consistent with this. In both states the dissipation is essential in that it controls the down stream propagation of energy from the mountain.

If the fluid was non-viscous, any wave produced by a westerly flow across the orography would grow to such an amplitude that the westerly flow would be ultimately reversed, and thus no down-stream propagation of wave energy could take place.

[1] Contribution no. 519.

This property of a non-viscous, orographically forced barotropic model has been demonstrated by Frederiksen (1982). He shows that the time-averaged zonal flow across the orography must be easterly. The time average is defined as the statistical-mechanical equilibrium of the model. If dissipation is present, the wave energy generated by a westerly flow may be absorbed downstream of the mountain and we can thus have a westerly time-averaged zonal flow which is what we observe in the atmosphere.

In the limit of weak dissipation, we may thus find results which differ radically from the statistical-mechanical equilibrium of Frederiksen (1982). On the other hand, the dissipation may be too weak to maintain a steady equilibrium of the model and the bifurcation described earlier may not be present. An increase of the dissipation can lead to a reappearance of the bifurcation, but we also know that if the dissipation is too strong the fluid will settle down into one stable and steady equilibrium. The purpose of the present study is to investigate different types of behaviour as the dissipation time scale is varied. We will concentrate on a range of parameter values for which no multiplicity of steady states has been found. Instead, a hysteresis-like effect will be demonstrated and this hysteresis effect is due to the same mechanism as the one creating the bifurcation. It will be argued that the hysteresis effect is perhaps the one most relevant to the atmosphere.

2. The model

A barotropic, balanced model on a spherical geometry is used as the main research tool in this investigation. The model is written in a spectral form and was originally developed by Hoskins and Simmons (1975). Throughout all numerical experiments, we will use a triangular truncation at wavenumber 42 and a leap frog time stepping scheme. The integration domain is global.

The governing equation of the model can be written

$$\frac{\partial \zeta}{\partial t} + J(\psi, \zeta + 2\sin\varphi + h) = \varepsilon(\zeta_E - \zeta). \qquad (1)$$

The vorticity ζ is a function of longitude (λ), latitude (φ) and time (t). The stream function ψ is defined through $\zeta = \nabla^2 \psi$ and h is a parameter incorporating the orographic effects. Assuming that eq. (1) is written in a non-dimensional form, h may be related to a dimensional mountain height (z) through the following equation (see Källén, 1981).

$$h = A\frac{z}{H}, \qquad (2)$$

where A is of order unity and H is the scale height of the atmosphere. The flow is driven by a vorticity forcing ζ_E and together with the dissipation term it acts as a Newtonian forcing on the right-hand side of eq. (1). The vorticity forcing will be applied to only one spectral component, namely the one describing a solid body rotation of the whole atmosphere around the earth's axis. As a measure of this forcing, we will use the zonally-averaged wind at 55° N latitude and this measure will be called u^*. The response of the model in terms of the zonally averaged wind at 55° N will be called u.

The time scale of the Newtonian forcing is determined by $1/\varepsilon$ which also is our dissipation time scale. The model behaviour will turn out to be sensitive to the dissipation time scale. For strong dissipation (short dissipation time scale) the model flow will quickly settle into an equilibrium and changes in the external conditions (h or ζ_E) will very quickly be adjusted to. When the dissipation is weak, the model response is more sluggish; a change in h or ζ_E will create transients which take a long time to die out. Which numerical value for $1/\varepsilon$ that should be chosen to represent atmospheric flow is difficult to judge. One may argue that a barotropic model should represent the vertically-averaged flow, and $1/\varepsilon$ can then be interpreted as the characteristic residence time of kinetic energy in the atmosphere. Data studies (Kanamitsu, 1981) then give a dimensional value of $1/\varepsilon$ of around 5 days. On the other hand, one can choose the barotropic flow to represent the flow at a given level, say 300 mb (Held, 1983), and then the dissipation is much weaker. A characteristic value of $1/\varepsilon$ would then be around 20 days. The main reason for choosing the 300 mb level is that the flow at this level is the most representative one for horizontal wave propagation. In the experiments described here, we will show results for both strong and weak dissipation (5 and 20 days time scale, respectively).

The orographic forcing is chosen as a single hump mountain profile which is confined to the mid-latitudes of one hemisphere (see Fig. 1). For simplicity, we choose the vorticity forcing to be in only one spectral component, namely the one

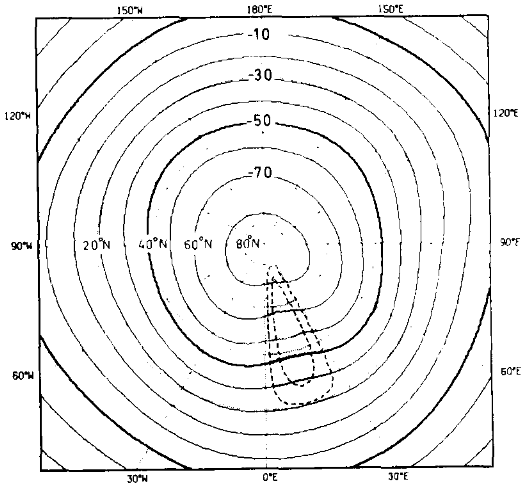

Fig. 1. Isolines of the stream function in arbitrary units. Dashed lines indicate the orography profile. The flow in this figure is in quasi-equilibrium when the zonal flow is at its minimum value and the dissipation time scale is 20 days. Maximum height of orography $h = 0.2$.

which describes a solid body rotation of the whole atmosphere. Through the orographic drag, the model response zonal wind will not be in solid body rotation but instead it will have a noticeably sharpened gradient south of the orography and be weakened in mid-latitudes. There will also be an unrealistic maximum in the zonal wind at the equator, which is due to the solid body rotation forcing. As we are mostly interested in the behaviour of the model at mid-latitudes, we will assume that this feature has no direct consequences for the mid-latitude behaviour. The short waves generated by the mountain will, to a large extent, be reflected due to the sharpened zonal wind gradient just south of the mountain while the longer waves can freely propagate into the southern hemisphere. The wind maximum at the equator thus prevents the shorter waves from propagating away from the source region while the longer waves are unaffected. The long waves may therefore become global modes, but as there is no source region in the southern hemisphere, they will be damped by dissipation. It is then a question of whether they are damped on the same time scale as they propogate to the southern hemisphere or if a global resonance may occur in the model? Some hemispheric experiments with a wall at the equator have been performed with the same type of forcing to investigate this. These hemispheric experiments showed a strong amplification of the long waves and thus it seems that the addition of another hemisphere mainly acts to damp out the large-scale modes. Therefore we do not expect global resonances to be of importance for the phenomena studied here.

Model simulations will be performed as time integrations where the zonal flow forcing is slowly varied. The zonal flow variations will produce variations in the response to the orography and the response will depend on the magnitude of the zonal flow. To investigate which characteristics of the flow that give rise to the rapid fluctuations observed, we have also looked at the eigenmodes of the model for some flow states. We calculated the eigenmodes by linearizing the model around a given flow state. The flow states used here are the ones produced by the time integration of the model. We thus investigate the linearized tendency of the model at a certain time instant. Numerically this is done by using the computation of the time tendency in the model. Assume that the model equation can be written as follows

$$\frac{\partial \zeta}{\partial t} = f(\zeta; h, \varepsilon). \tag{3}$$

The function f includes both linear and non-linear terms in eq. (1). The rewritten model eq. (3) may now be linearized around a certain flow state ζ_0, if we assume $\zeta = \zeta_0 + \zeta'$, where

$$|\bar{\zeta}'| < |\bar{\zeta}_0|, \quad \text{and} \quad \left|\frac{\partial \bar{\zeta}_0}{\partial t}\right| < \left|\frac{\partial \bar{\zeta}'}{\partial t}\right|.$$

The overbar denotes an area integrated value. The first condition simply says that the perturbation should be small compared with the basic state. The second condition implies that the time evolution of the basic state should be slow when compared with the growth rate of the disturbance. The largest eigenvalue should thus be large compared with the inverse of the evolution time scale of the flow at the time instant where the computation of the eigenmodes is performed. If this is not so, it is difficult to give a meaningful interpretation to the structure of the most unstable eigenmode. We will return to this problem when discussing the results.

As noted previously, our model is written in a spectral form where all space-dependent variables are expanded in a sum of spherical harmonics, Y_i

$$\zeta = \sum_i \zeta_i(t)\, Y_i(\lambda, \varphi). \tag{4}$$

The complex amplitudes ζ_l are now split up into their real and imaginary parts and the state of the model may instead be described by a real vector. The elements of the real vector $\boldsymbol{x}$ are thus given by the real and imaginary parts of ζ_l as follows

$$x = (\mathrm{Re}(\zeta_0), \mathrm{Im}(\zeta_0), \ldots, \mathrm{Re}(\zeta_l), \mathrm{Im}(\zeta_l), \ldots). \tag{5}$$

With this real state vector, we can write our model eq. (3) as

$$\dot{\boldsymbol{x}} = \boldsymbol{g}(\boldsymbol{x}; h, \varepsilon). \tag{6}$$

The vector function $\boldsymbol{g}$ corresponds to the function f in (3). The components of $\boldsymbol{g}$ are given by the real and imaginary parts of f projected on each spectral component of the expansion (4). We can now determine the linearized form of our model by perturbing each component of $\boldsymbol{x}$ separately and project this response on each of the spectral components. This may be done numerically by calculating the model tendency for one time step when the real or imaginary part of a spectral component is perturbed.

The resulting linearized model may be written

$$\frac{\mathrm{d}x_i'}{\mathrm{d}t} = \frac{\partial g_i(\boldsymbol{x}_0; h, \varepsilon)}{\partial x_j} x_j' \tag{7}$$

The elements in the matrix defining the linearized time evolution are thus given by $\partial g_i/\partial x_j$. We use a numerical procedure to find the eigenvalues and the eigenmodes and we will look at the fastest growing mode, i.e., the one with a maximum in the real part of the eigenvalue. For reasons of computer economy and efficiency, we have limited the truncation to total wavenumber 21 when determining the eigenmodes.

If the eigenvalue of the fastest growing mode is real, the corresponding eigenvector is also real and the amplitudes obtained in the eigenvector can be used directly to determine the structure of the fastest growing mode. If the eigenvalue has an imaginary part, the corresponding eigenvector must also be imaginary (the matrix in eq. (5) only has real elements) and the interpretation in terms of vorticity amplitudes is not so straightforward. However, we know that imaginary eigenvalues must appear in complex conjugated pairs as the coefficients of the eigenvalue equation are real. The eigenvectors of complex conjugated eigenvalues are also complex conjugated. To describe a real valued solution, we thus add the conjugated eigenmodes to obtain

$$\begin{aligned} x_k &= A\mathrm{e}^{\mathrm{Re}(\lambda_j)t}\,(\mathrm{e}^{i\mathrm{Im}(\lambda_j)t}\,y_{jk} + \mathrm{e}^{-i\mathrm{Im}(\lambda_j)t}\,y_{jk}^*) \\ &= A\mathrm{e}^{\mathrm{Re}(\lambda_j)t}\,(\cos\,(\mathrm{Im}(\lambda_j)t)\,\mathrm{Re}(y_{jk}) \\ &\quad - \sin\,(\mathrm{Im}(\lambda_j)t)\,\mathrm{Im}(y_{jk})), \end{aligned} \tag{8}$$

where x_k is the kth component of the modified state vector $\boldsymbol{x}$. The amplitude A is arbitrary and y_{jk} is the kth component of the jth eigenvector belonging to the eigenvalue λ_j. Both λ_j and y_{jk} are complex, all other variables are real (a complex conjugate is denoted by an asterisk).

From eq. (8), we see that the structure of the combined eigenmode is time-dependent in a periodic manner. To judge the physical significance of the structure, we may either look at the amplitude envelope of the mode or we can look at the structure at a given time. The most natural time is $t = 0$ as the linearization procedure implies that we are interested in the initial tendencies. The structure at $t = 0$ is given by the real part of the eigenvector components as can be seen from eq. (8). In the following, we will only study the real part of the eigenvector amplitudes and the structures shown are thus relevant for the initial development. We thus wish to interpret the structures as quickly developing perturbations on a slowly evolving state.

3. Results

To set up an initially balanced flow, we start an integration with a constant forcing and a solid body rotation of the atmosphere which equals the forcing. The orography will cause a weakening of the zonal flow in mid-latitudes and a downstream wave pattern will develop. We integrate the model over about one dissipation time scale to achieve an almost balanced state (see Fig. 1 for structure of mountain and initial flow). The zonal flow forcing is then slowly increased such that the ratio between the doubling time of the forcing and the dissipation time scale is 5/1. We thus assume that the flow is in a quasi-stationary equilibrium most of the time, an assumption that will be partly verified with the eigenmode analysis later. After having reached a forcing which is 2.25 times its original value, we reverse the slow increase of the forcing to a slow decrease and return to the original value of the forcing. The results of two such experiments are

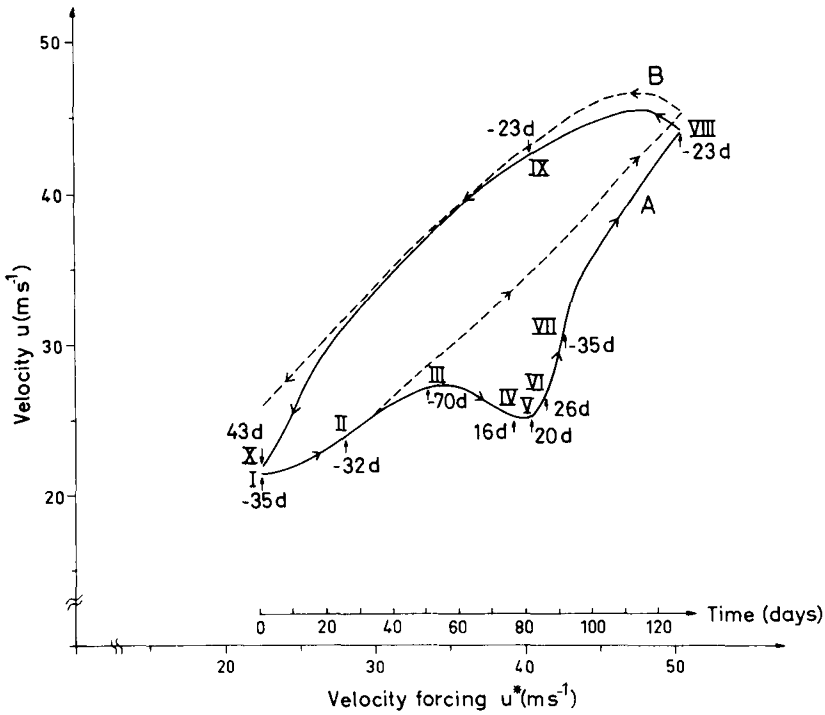

Fig. 2. Corresponding values of forcing (u^*) and response (u) of the zonally-averaged flow at 55° N for an increasing and decreasing zonal forcing. Dashed lines correspond to a dissipation time scale of 5 days (curve B), full lines 20 days (curve A). Points I–X indicate where the growth rate of the most unstable eigenmode has been determined. The inverse of the growth rate in units of days is also indicated in the figure. Negative values imply stability. The time scale at the bottom of the diagram refers to the rate of increase of u^* in curve A.

shown in Fig. 2. The quantities plotted in Fig. 2 are the zonally averaged forcing and response of the zonal flow at latitude 55° N, i.e. close to the mountain peak. The results of two different experiments are displayed, one with a dissipation time scale of 5 days (curve B) and the other with a time scale of 20 days (curve A). All other flow parameters are identical.

The hysteresis effect in curve B is not very marked, the zonal flow follows the increase and decrease of the forcing with a certain time lag. Curve A shows a much stronger hysteresis effect and in fact for the solution branch where the forcing is increasing we have a slow decrease and a subsequent sharp increase of the zonal flow. The decrease appears to be smooth and gentle while the increase is abrupt and also contains some small oscillations. This points to an instability occurring for some critical value of the zonal flow. When the same value of the zonal forcing is reached on the descending branch, we do not observe this jump and thus we have a marked hysteresis effect. Instead, we find a weak jump close to the left-hand side of the figure where the zonal flow forcing has returned to its original value. To judge the stability/instability of each flow state, a linear eigenmode analysis was performed for some of the flow states in the time integration. The linear growth rate of the fastest growing mode is marked in Fig. 2 for some points along curve B. On the slowly varying parts, the growth rate is always negative, thus indicating a quasi-balanced flow. At the two jumps observed, one on the ascending branch (point V) and one on the descending branch (point X), we have positive growth rates and thus an instability of the flow.

The hysteresis effect and the instabilities point to the existence of multiple steady-states and two stable solution branches separated by an unstable steady-state (see Källén, 1982). This hypothesis was tested by starting integrations from two initial

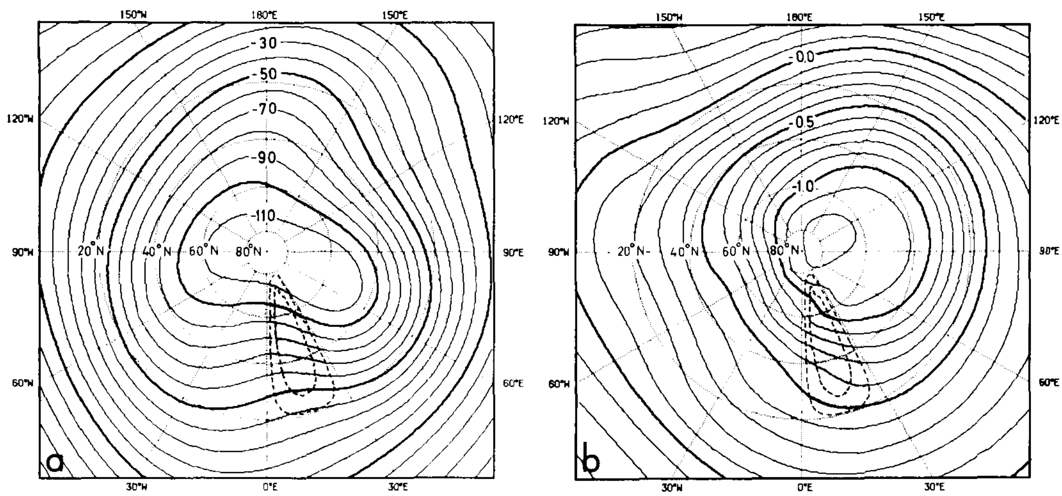

Fig. 3.(a) Flow field corresponding to point *V* on the full curve in Fig. 2. Stream function units are the same as in Fig. 1.(b) Structure of the most unstable eigenmode for the flow field in (a). Amplitude of the stream function is arbitrary.

states having the same forcing but on the two different branches of curve A in Fig. 2 (points V and IX). It was then found that both integrations evolved to the same state, situated somewhere intermediate between the two branches. The time scale of evolution to this intermediate state is slower than the time scale of the jump between points V and VII in Fig. 2. No multiple steady-states were thus found with this present choice of orography and this might seem to indicate that the CdV blocking theory is not very relevant for atmospherically realistic flow parameters.

By looking at individual flow patterns, we may, however, trace some of the qualitative features discussed in the introductory section of this paper. We first look at the flow just at the onset of the instability. The flow corresponding to point V on curve A is shown in Fig. 3a. In Fig. 3b, the structure of the most unstable eigenmode is also shown for the same flow situation as in Fig. 3a. We see a clear wave drag pattern, where the flow trough is roughly 90° phase-shifted downstream relative to the mountain, and we thus have a very large wave-drag. The zonal flow is close to its minimum value (Fig. 2) and the unstable eigenmode has a growth rate of $1/20\ \mathrm{days}^{-1}$.

The occurrence of a growing eigenmode shows that the flow is about to change rapidly (i.e. it is not anymore in a quasi-stationary state). The structure of the fastest growing mode gives an indication of the physical mechanism behind this growth. In Fig. 3b, we see a sharp gradient across the mountain and this shows that the mountain drag or push causes the flow to change. As the sign of the eigenmode is arbitrary, we cannot determine whether it is a push or a drag, but knowing that an increase in the zonal flow will follow, we can deduce that it has to be a push. The arbitrary sign of the eigenmode in Fig. 3b is therefore chosen to give a trough on the windward side of the mountain.

The next flow situation (Fig. 4) is after the zonal flow has passed its minimum value and is increasing rapidly. The flow (Fig. 4a) is now much more symmetric around the mountain and there is thus a marked decrease in the wave drag. The unstable eigenmode (Fig. 4b) also shows a symmetric structure around the mountain, i.e., the mountain push/drag is small. This is consistent with the fact that we have almost reached a quasi-stationary state again. We must, however, be careful in interpreting the structure of the eigenmode, as the rate of change of the flow at point VII in Fig. 2 is rather large and the linearized analysis may therefore not be valid here. In any case, it is clear from these flow pictures that the dip and subsequent rapid increase of the zonal flow shown in curve A in Fig. 2 is due to orographic effects which are qualitatively similar to the ones which act when multiple flow equilibria are found (CdV). However, it is not possible to maintain such an equilibrium in this

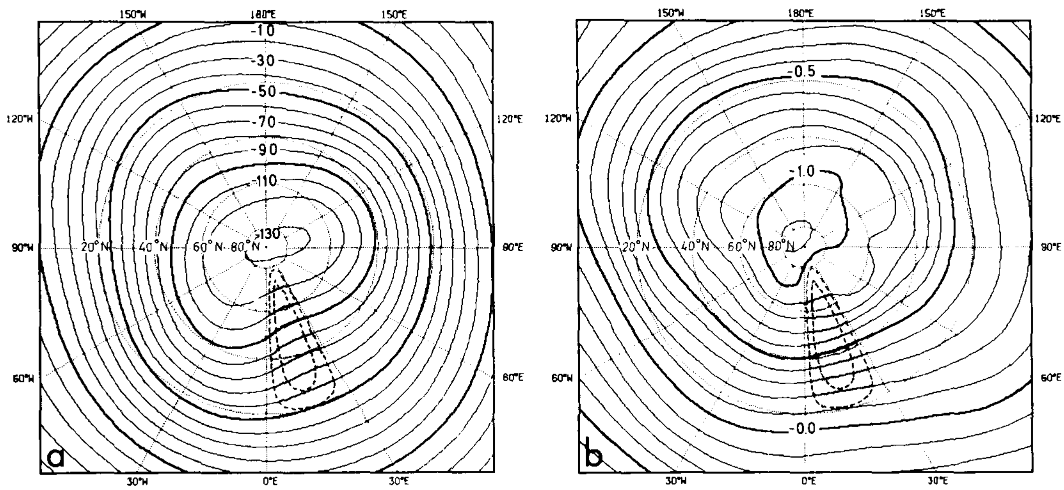

Fig. 4. Same as in Fig. 3 but here for point no. VII in Fig. 2. Stream function units are the same as in Fig. 3.

model, as the wave energy generated by the mountain is dispersed and dissipated over the entire sphere. The qualitative phenomena can only be found as a transient effect when there is a gradual change of the zonal flow. For an increasing zonal flow we see this effect quite clearly and also for a decrease in the zonal flow we observe a weak jump "back" to the lower branch of curve A in Fig. 2 at point X. Fig. 5 shows the flow at point X and we can see that there is a large amplitude trough across the orography and that a large-wave amplitude flow is being re-established.

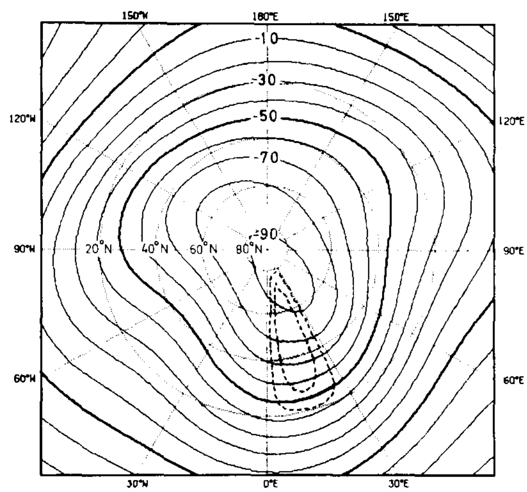

Fig. 5. Flow field at point no. X in Fig. 2. Stream function units are the same as in Fig. 1.

4. Conclusions

The hysteresis-like effect found in the model integrations performed shows a clear qualitative resemblance to the multiple equilibrium theory originally proposed by CdV. There is, however, one very important difference, namely, that the two different stable response modes only appear as transient phenomena. They can thus be said to be quasi-balanced: an increasing or decreasing zonal flow is required to maintain the balance. The instability occurring at a critical value of the zonal flow is triggered by the orography; without the orography present no waves would be generated and if we remove the orography and calculate the eigenmodes at any of the flow states given in Fig. 2, we find that they are all unstable with growth rates of $\mathcal{O}$ (10 days^{-1}). The orographically generated instability occurs when the zonal flow increases above a certain critical value and if the dissipation is sufficiently weak. The hysteresis loop is in the region of a resonant value of the zonal wind and this in turn depends on the spatial structure of the waves set up by the orography. For a periodically-varying zonal forcing, the strength of the hysteresis behaviour is continuously dependent on the dissipation rate, the height of the orography and the time rate of change of the zonal forcing. The behaviour described is thus not hysteretic in a strict sense. If the time rate of change of the forcing is very long compared to the dissipation time scale, there will be no loop like the one shown in Fig. 2. Instead we would find a single curve both for the increasing and decreasing forcing. To find hysteresis effects in the strict sense, we must require a bifurcation of the steady-state solutions. However, due to the structure of the loops in Fig. 2, we still wish to call it a hysteresis in analogy with ferromagnetic phenomena. The main point is that the steady behaviour may not be all that relevant to the atmosphere on a time scale of a few weeks when there is a forcing which is changing on the time scale of a season.

For an understanding of why it is not possible to maintain two different stable equilibria for the parameter values chosen in this study, we may refer to wave propagation theory (Hoskins and Karoly, 1981). The short waves generated by the orography are mainly trapped in the hemisphere where they are generated, while a considerable part of the long-wave energy propagates through to the other hemisphere where it is eventually dissipated. Experiments with the flow confined to one hemisphere have shown a very strong amplification of the long waves in the generation hemisphere and in this case we can maintain multiple equilibria with a reasonable orographic forcing (Källén, 1982). In the atmosphere, we can have propagation of long-wave energy between the hemispheres and it is therefore not very realistic to assume that a long-wave resonance can be maintained for any length of time. The mechanism found in this study, i.e., a transient hysteresis effect, seems more realistic, in particular as the time scale of the increase/decrease in the forcing is around 100 days (a season). The mechanism underlying the transition between the two solution branches is similar to the one responsible for the bifurcation in the steady-state problem and the qualitative conclusions are therefore the same. The long-wave response of the atmosphere may be in one of two different states; which one prevails depends on the time history of the zonal mean flow.

In a barotropic model, we have to specify an external momentum source, and this serves as a crude parameterization of the most fundamental energy-generating mechanism in the atmosphere, namely the differential heating. The intricate balance which maintains the zonal flow in mid-latitudes should also be taken into account in studying hysteresis effects and it should be the differential heating rather than the zonal flow forcing which is varied. Another major factor is the existence of baroclinically unstable waves which contribute to the forcing of the large-scale waves: the baroclinic instability is in turn governed by the differential heating gradient and we thus have a coupling between the hysteresis effect and baroclinic instability. Earlier studies of this (Charney and Strauss, 1980; Reinhold and Pierrehumbert, 1982; Källén, 1983) have mainly considered the multiple equilibrium or regime equilibrium problem and thus required some steady, resonant behaviour. Due to the range of time scales involved, it would perhaps be more realistic to consider this as a hysteresis problem and to look for rapid transitions when there is a slow change in the external driving forces.

5. Acknowledgements

I wish to thank Jørgen Frederiksen and Åke Johansson for many fruitful discussions on the subject of this paper. The computer simulations were made on the ECMWF computers and I thank Adrian Simmons for making the barotropic model available to me. The computer time was made available through use of time allocated to the Swedish Meteorological and Hydrological Institute (SMHI) and the research project is supported by the Swedish Natural Science Research Council grant no S-FI 1705–100.

REFERENCES

Charney, J. G. and De Vore, J. G. 1979. Multiple flow equilibria in the atmosphere and blocking. *J. Atmos. Sci. 36*, 1205–1216.

Charney, J. G. and Strauss, D. M. 1980. Form drag instability, multiple equilibria and propagating planetary waves in baroclinic, orographically forced, planetary wave systems. *J. Atmos. Sci. 37*, 1157–1176.

Davey, M. K. 1980. A quasi-linear theory for rotating flow over topography. Part I: Steady β-plane channel. *J. Fluid Mech. 99*, 267–292.

Davey, M. K. 1981. A quasi-linear theory for rotating flow over topography. Part II: Beta-plane annulurs. *J. Fluid Mech. 103*, 297–320.

Frederiksen, J. S. 1982. Eastward and westward flows over topography in non-linear and linear barotropic models. *J. Atmos. Sci. 39*, 2477–2489.

Held, I. M. 1983. Stationary and quasi-stationary eddies in the extra-tropical troposphere: theory. In: *Large-Scale dynamical processes in the atmosphere*, ed. B. Hoskins and R. P. Pearce. Academic Press, p. 127–168.

Hoskins, B. J. and Karoly, D. J. 1981. The steady linear response of a spherical atmosphere to thermal and orographic forcing. *J. Atmos. Sci. 38*, 1179–1196.

Hoskins, B. J. and Simmons, A. J. 1975. A multilayer spectral model and the semi-implicit method. *Q. J. R. Meterol. Soc. 101*, 637–655.

Källén, E. 1981. The non-linear effects of orographic and momentum forcing in a low-order barotropic model. *J. Atmos. Sci. 38*, 2150–2163.

Källén, E. 1982. Bifurcation properties of quasi-geostrophic models and their relation to atmospheric blocking. *Tellus 34*, 255–265.

Källén, E. 1983. A note on orographically-induced instabilities in two-layer models. *J. Atmos. Sci. 40*, 500–505.

Kanamitsu, M. 1981. Some climatological and energy budget calculations using the FGGE III-b analyses during January 1979. In: *Dynamic meteorology; data assimilation methods*, ed. L. Bengtsson, M. Ghil, E. Källén. Springer Verlag, pp. 263–318.

Reinhold, B. B. and Pierrehumbert, R. T. 1982. Dynamics of weather regimes: quasi-stationary waves and blocking. *Mon. Wea. Rev. 110*, 1105–1145.